Journal of Building Engineering 111 (2025) 113348

Contents lists available at ScienceDirect

Journal of Building Engineering

journal homepage: www.elsevier.com/locate/jobe

Full length article

Experimental investigation of edge distance effects on uplift response in OSB sheathing-to-framing nailed connections using digital image correlation

Georgios Tsampras [a,*,1], Richard Zabel [b,2], Kaixin Chen [a,3]

[a] Department of Structural Engineering, University of California San Diego, United States of America
[b] Mulhern and Kulp, United States of America

ARTICLE INFO

Keywords:
Digital image correlation
Full-field strain data
Nailed connections
Light-frame wood buildings
Experimental testing

ABSTRACT

Nailed connections between Oriented Strand Board (OSB) structural sheathing panels and wood sill plates are commonly used to form panel wall assemblies for light-framed wood buildings in the United States. The structural integrity of light-framed wood buildings depends on the structural performance of OSB sheathing-to-framing nailed connections. This paper characterizes experimentally the effect of the distance between the OSB panel edge and the nails on the uplift response of sheathing-to-framing nailed connections. Four edge distances were considered. Twelve OSB sheathing-to-framing nailed connections were tested to failure. Analysis of the three-dimensional displacement and strain fields computed using state-of-the-art digital image correlation method was performed to provide insights into the force–displacement response, the yield mechanism, the post-yielding response, the failure mechanisms, and the evolution of stiffness of the connections. Reduction of the nail edge distance resulted in a reduced maximum deformation capacity of the sheathing-to-framing nailed connections without affecting significantly the uplift force capacity. The uplift yield force and yield displacement was effectively independent of the edge distance. It is shown that the yield force can be estimated assuming a nail bearing pressure distribution that is justified based on experimental observations. Effectively no strain localization and stiffness degradation was observed up to an uplift force equal to the uplift design force computed using the American National Design Specification. Initiation of non-uniform strain localization was observed at uplift force larger than the yield force of the connections. Two failure modes that depend on the nail edge distance were observed at the end of the tests.

1. Introduction

Wind-induced loads acting on light-framed wood buildings result in lateral and uplift forces resisted by structural panel wall assemblies. The force and displacement capacity of a light-framed panel wall assembly is primarily controlled by the force–displacement response of the connections between the Oriented Strand Board (OSB) sheathing panel and the wood framing. Fig. 1

* Corresponding author.
E-mail address: gtsampras@ucsd.edu (G. Tsampras).
URL: https://tsampras.ucsd.edu (G. Tsampras).
[1] Assistant Professor.
[2] Project Manager and Director of Engineering.
[3] PhD Student.

https://doi.org/10.1016/j.jobe.2025.113348
Received 2 November 2024; Received in revised form 24 June 2025; Accepted 27 June 2025
Available online 12 July 2025
2352-7102/© 2025 The Authors. Published by Elsevier Ltd. This is an open access article under the CC BY-NC-ND license (http://creativecommons.org/licenses/by-nc-nd/4.0/).

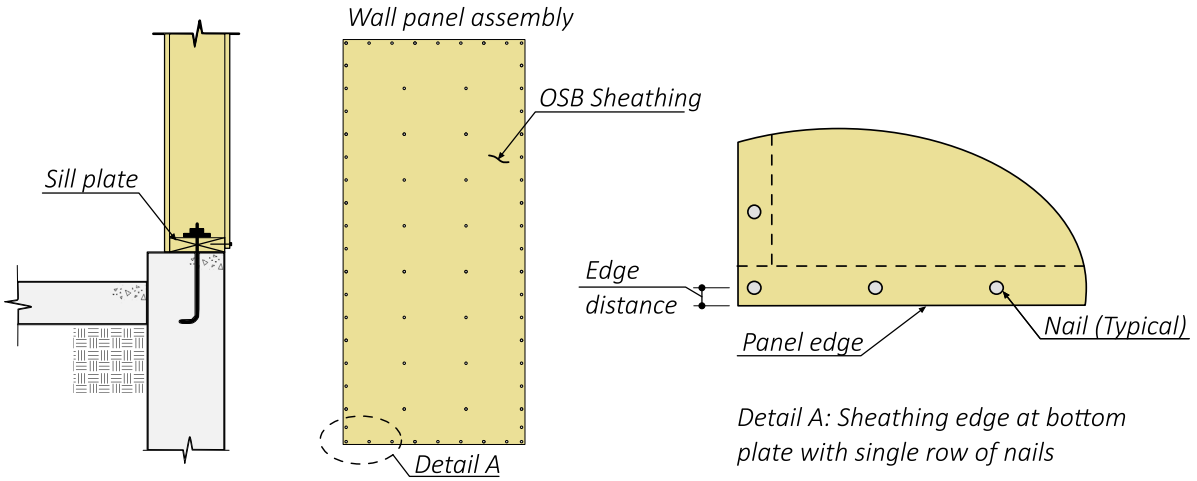


Fig. 1. Schematic representation of a panel wall assembly and the Oriented Strand Board sheathing-to-framing nailed connection in a typical light-framed wood building.

shows a schematic representation of a structural panel wall assembly and OSB sheathing-to-framing nailed connections in a typical light-framed wood building. Detail A in Fig. 1 shows the use of a single row of nails to connect the OSB panel to the bottom wood sill plate of a structural wall panel assembly.

Researchers have studied the effect of various construction and aging parameters on the force–displacement response of sheathing-to-framing connections. The following paragraphs list specific examples of studies. Despite the broad range of published studies, it is shown that there is need for detailed research on the effect of the edge distance on the wind-induced uplift response of sheathing-to-framing connections using state-of-the-art research methods.

Easley et al. [1] provided formulas for the analysis of typical wood-frame structural wall panel assemblies with sheathing attached by nails or other types of discrete fasteners. The formulas were modified versions of formulas developed for corrugated metal diaphragms. Results from experimental tests were used. Localized deformations at the location of the nails were visually observed but no measurements were made.

Dolan and Madsen [2] studied the effect of the timber and nail materials on the monotonic and cyclic force–displacement characteristics of the sheathing-to-framing connection response. The authors suggested that the understanding of the response of the sheathing-to-framing connections is required for the further understanding of the global response of wall assemblies. Salenikovich and Dolan [3,4] conducted a comprehensive study to assess the monotonic and cyclic racking performance of panel wall assemblies with various aspect ratios.

Fonseca et al. [5] assessed experimentally the force–displacement response of nail, wood screw, and staple fastener connections under monotonic and cyclic loads as part of the CUREE-Caltech Woodframe Project. A broad range of parameters were assessed with the goal to calibrate numerical models. For example, the effect of the nail penetration in nailed connections was assessed. Reduction in the force and displacement capacity of wall assemblies was observed due to overdriven nails in the sheathing-to-framing connections [6]. Fonseca et al. [5] also conducted tests with identification numbers 85, 87, 89, 97, and 99 to assess the effect of edge distance in the force–displacement response of the single-nail connections. The authors did not report detailed and conclusive results on the effect of the edge distance on the force–displacement response of the nailed connections [5].

Kent et al. [7] studied the effect of cyclic degradation of wood on the force–displacement response of sheathing-to-framing connections. The monotonic and cyclic response of sheathing-to-framing connections and panel wall assemblies has been also studied considering different thicknesses of OSB panels and different lengths and diameters of nails by Seim et al. [8], Sartori and Tomasi [9]. The authors observed that the in-plane behavior of panel wall assemblies strongly depends on the sheathing-to-framing connections. The authors used the experimental results to calibrate numerical models of the wall assemblies developed by Folz and Filiatrault [10]. Zhou et al. [11] investigated the influence of the thickness of the middle member in double-shear nailed connections. Experimental results indicated that if the nail penetration length is greater than five times the nail diameter, no reduction in lateral resistance of double-shear nail joints should be expected.

The dependence of the force–displacement response of OSB sheathing-to-framing nailed connections to the bidirectional displacement loading protocol was assessed by Bader et al. [12]. The bidirectional path of the displacement loading protocol affected the shape of the resultant force–displacement response but it had limited effect on the peak resultant force capacity of the connection.

Way et al. [13] experimentally studied the weathering effects associated with moisture degradation on the lateral force–displacement capacity of wall assemblies with sheathing-to-framing nailed connections. The authors concluded that wall assemblies with weathered OSB sheathing panels had reduced shear force capacity compared to non-weathered OSB sheathing panels. However, the reduction of shear force capacity of the weathered wall assemblies was found to be within 10% of the design shear force level.

The effect of the intermediate insulation layer on the overall lateral resistance of the sheathing-to-framing nailed connections was studied by Spasojevic et al. [14]. The authors conducted experimental and analytical studies which demonstrated that the insulation has a significant impact on the lateral resistance of sheathing-to-framing nailed connections.

Based on the literature review, it is concluded that researchers have already studied the effect of various construction and aging parameters on the force–displacement response of sheathing-to-framing connections, such as nail penetration, member thickness, and moisture induced degradation. Supplemental detailed studies that experimentally assess the simulated wind-induced uplift force effects on the OSB sheathing-to-framing nailed connections with varying nail edge distance are still required to be conducted using state-of-the-art research methods. The results of these studies could enhance the confidence in the design of light-framed wood buildings with nail edge distance that may deviates from the design requirements due to construction imperfections.

2. Scope and aim of research

The in-depth understanding of the nailed connection uplift response is required prior to conducting a detailed assessment of the wall panel assembly response subjected to combined horizontal and uplift loads. As a result, this study characterizes experimentally the effect of the distance between the OSB structural sheathing panel edge and the nails on the uplift response of OSB sheathing-to-framing nailed connections. Four edge distances were considered. Twelve OSB sheathing-to-framing nailed connections were constructed and tested to failure. Detailed analysis of the full-field three-dimensional displacements and strains computed using three-dimensional Digital Image Correlation (DIC) technique was performed to provide insights into the force–displacement response, the yield mechanism, the post-yielding response, the failure mechanisms, and the evolution of stiffness of the connections.

The aim of this study is to use state-of-the-art data collection and analysis methods to generate detailed experimental observations on the effect of edge distance on the uplift response of nailed connections, relevant to structural engineering practice. Importantly, this research does not seek to alter code-defined edge distance requirements but to provide insights into the performance of light-framed wood buildings with nail edge distances that may deviate from design requirements due to construction imperfections.

The effects of aging and other construction parameters on connection behavior are outside this study's scope. Future research should experimentally assess the full-field displacement and strain response of wall panel assemblies under combined horizontal and uplift loads, employing advanced data collection and analysis techniques.

3. Experimental methods

3.1. Design considerations

Section 12.1.2.1 of the National Design Specification (NDS) [15] defines *Edge Distance* as the distance from the edge of a member to the center of the nearest fastener, measured perpendicular to grain. The Special Design Provisions for Wind and Seismic (SDPWS) load effects published by the American Wood Council (AWC) [16], defines *End Distance* as the distance from the end of a member to the center of the nearest fastener, measured parallel to grain.

The allowable force capacity for the connections provided to resist wind-induced uplift forces can be determined using the procedures described in NDS for Wood Construction or using SDPWS. Chapter 12 of the 2018 NDS provides individual dowel capacities and the required adjustment factors, including but not limited to the minimum edge distance of four times the diameter of the dowel per Table 12.5.1C for the loaded edge. When a member is loaded perpendicular to the grain, the loaded edge shall be defined as the edge in the direction toward which the fastener is acting. Assuming nails with diameter $D = 2.87$ mm (0.113 inches) were utilized in panel wall assemblies, the required edge distances would be 11.48 mm (0.452 inches).

3.2. Test groups

Three specimens were tested in each one of the four test groups. Specimens in Test Group A were used to establish the baseline results, with edge distance equal to 38.1 mm (1.5 inches). Specimens in Test Group B were constructed using edge distance equal to 19.05 mm (3/4 inches). Specimens in Test Groups C and D were constructed using edge distances equal to $4D = 11.48$ mm and $2D = 5.74$ mm, respectively. Specimens in Test Groups A, B, and C satisfy the minimum required edge distance per NDS equal to $4D = 11.48$ mm.

A single row of five nails was used in the connections in all specimens. The allowable force capacity of Specimens in Test Groups A, B, and C per Chapter 12 of the NDS is $V_{NDS} = 2.0$ kN (448 lbf). The computation of the allowable force capacity assumes 5 nails with individual dowel capacity 0.25 kN/nail (56 lbf/nail) based on the values listed in NDS Table 12Q. The duration factor $C_d = 1.6$ is considered in the computation of V_{NDS}. The sill plate is assumed to be a Douglas fir plate with specific gravity $G = 0.5$. The NDS Table 12.5.1 A incorporates a 50% reduction in capacity for cases that edge distance requirements are not met. As a result, the allowable force capacity for the Specimens in Test Group D is determined to be $V_{NDS} = 1.0$ kN (224 lbf).

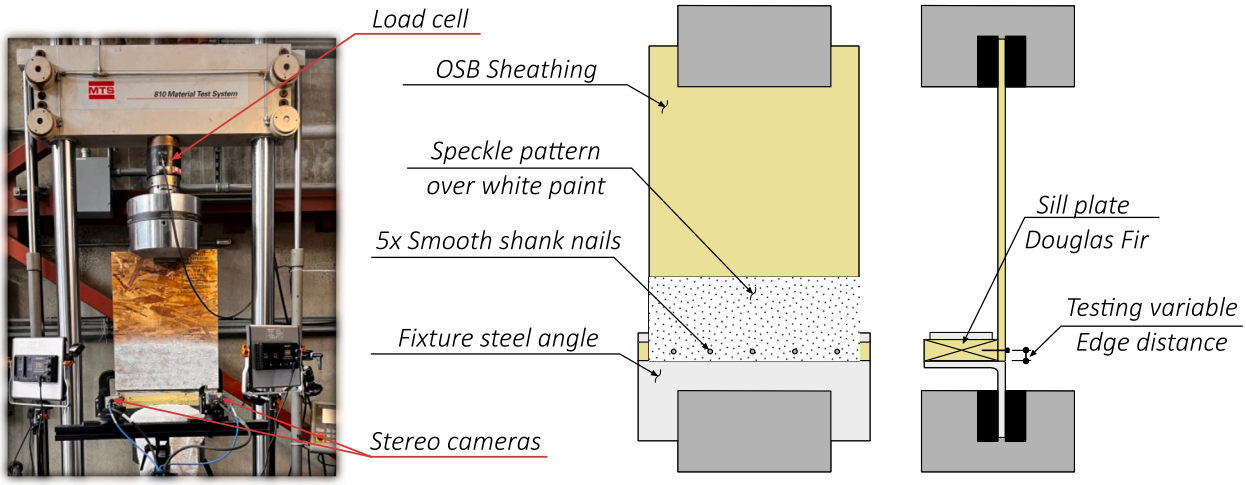


Fig. 2. Experimental setup.

3.3. Test setup

Fig. 2 shows the experimental setup developed for this study. OSB panels with 11.11 mm (7/16 inches) nominal thickness were used. The OSB panels were cut to 457.2 mm (18 inches) wide by 609.6 mm (24 inches) long dimensions. Five nails were used to connect the OSB panels to a Douglas Fir sill plate wood framing. The use of five nails allowed for studying (1) the effects of construction tolerances on the distribution of displacements and strains in the OSB panels close to the region of the nails with different edge distances, (2) the effects of multiple nails in lieu of a single nail test (group effects), (3) the redistribution of strain as progressive failure occurred in the nailed connection, and (4) the effects of the imperfections introduced by the position of each nail. The length and diameter of the nails were 60.325 mm (2.375 inches) and $D = 2.87$ mm (0.113 inches), respectively. Sill plate wood framing with actual dimensions 38.1 mm (1.5 inches) thick and 139.7 mm (5.5 inches) wide were used. The OSB sheathing-to-framing connection assembly was clamped to a steel angle section. The steel angle section was clamped by the hydraulic grip at the end of a hydraulic servo-controlled actuator. The hydraulic servo-controlled actuator was used to simulate the uplift effects on the connection by applying a monotonically increasing displacement-controlled motion with a velocity of 0.08 mm/sec.

Fig. 3 shows representative results on the difference between the actual nail edge distance relative to the target nail edge distance along with the associated percentage of the relative error in Specimens B2, B3, C2, C3, D2, and D3. The positional data were taken into consideration for the assessment of the uplift response of the connections and the strain localization in the OSB regions with nails. Specimens with actual edge distance different from the target edge distance were deemed acceptable and representative of construction practice.

3.4. Instrumentation and workflow

DIC technique was used in this test to quantify the full-field of displacements and strains on the specimens. To facilitate DIC data collection, a black speckle pattern was applied over white paint in the external face of the OSB sheathing panels near the nailed connections. Two Basler ace acA4112-30um cameras were used to collect images of the speckle pattern during testing. A Sony IMX253 monochrome camera sensor with a resolution of 12 megapixels (4096 pixels × 3000 pixels) and a maximum frame rate of 30 frames per second was used. The cameras used Schneider-Kreuznach JADE 2.8/25 C lenses with a focal length of 25 mm and a range of f-number (the ratio of a lens's focal length to its aperture diameter) from 2.8 to 16. The image data were stored in .tiff files and analyzed using DIC to compute the three-dimensional displacement and strain fields [17]. DIC allows for the assessment of the strain localization during the testing process. In addition to image data, total force and displacement data were collected using a load cell and a linear position sensor, respectively.

Fig. 4 shows the workflow of experimental testing and analysis of the collected data and metadata. Once a specimen was installed on the test setup, the MTS TestSuite™ [18] was utilized to execute the test sequence. After reaching the peak force response, the displacement continued increasing until 20% of the peak force was reached. The force and displacement data was collected using the data acquisition channels onboard the MTS controller. The force and displacement data were down-sampled and synchronized with the data acquisition system used to collect the stereo camera imaging data. The stereo camera imaging data were acquired using the software VIC-Snap [19]. The software VIC-3D [17,19] was used to perform the stereo camera calibration required to compute the intrinsic parameters for each camera and the extrinsic parameters of the pair of stereo cameras. Once calibration was completed, VIC-3D was used to analyze the sequence of stereo imaging data acquired during the test and compute the three-dimensional displacement field of the OSB panel where the speckle pattern was applied. The computation of the three-dimensional

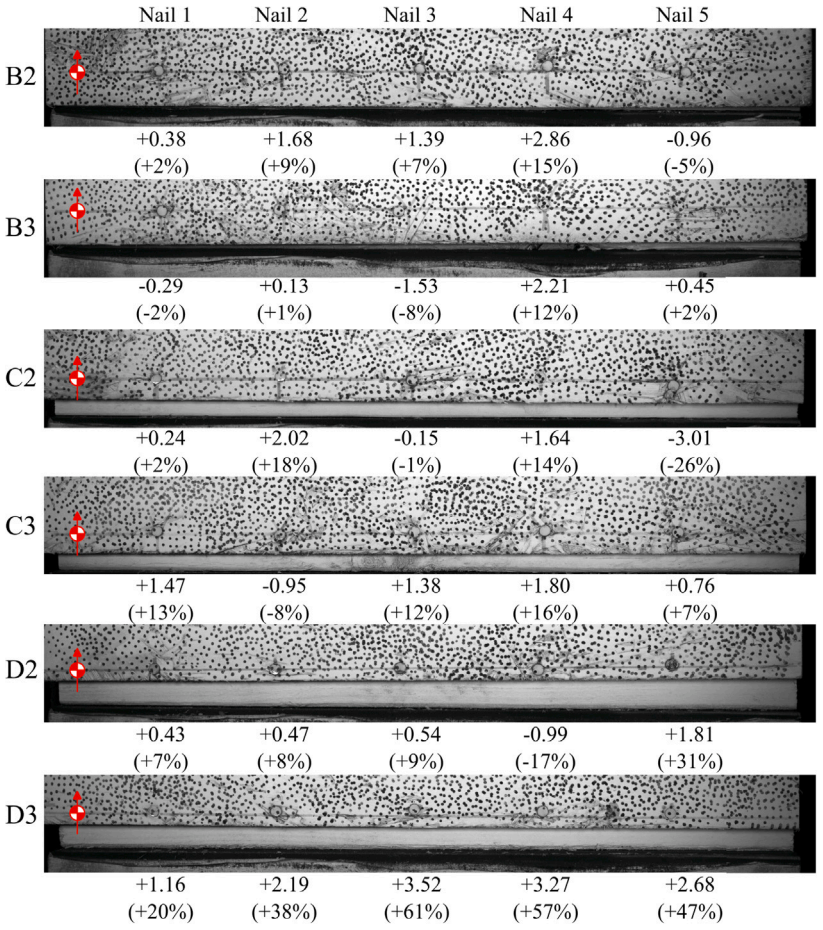


Fig. 3. Representative actual nail position relative to the target position in millimeters and the associated percentage of the relative error in Specimens B2, B3, C2, C3, D2, and D3.

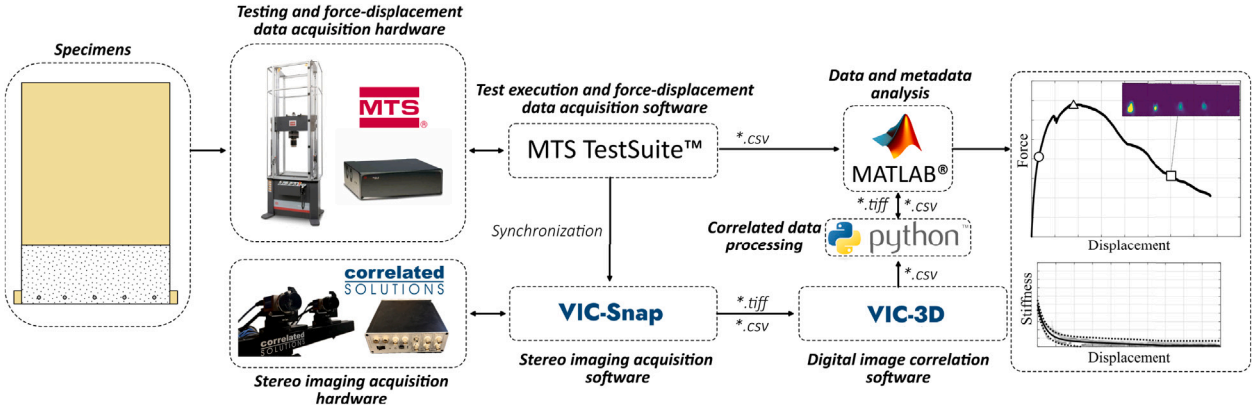


Fig. 4. Testing and analysis workflow.

displacement field allowed for the computation of the full-field engineering strain in the region of the speckle pattern. The data was further analyzed using MATLAB [20] and Python [21] to formulate conclusions on the effect of the edge distance on the uplift response of the OSB sheathing-to-framing connections at specific performance limit states.

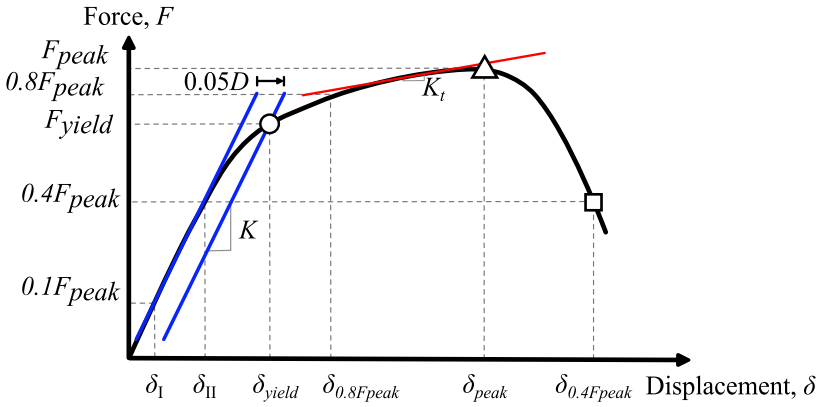


Fig. 5. Definition of engineering demand parameters using a schematic representation of an example force–displacement response. $0.05D = 0.144$ mm.

Table 1
Summary of response quantities.

ID [–]	Target edge distance [mm]	F_{yield} [kN]	δ_{yield} [mm]	F_{peak} [kN]	δ_{peak} [mm]	$\delta_{0.4F_{peak}}$ [mm]	K [kN/mm]
A1	38.10	3.25	1.23	5.95	8.86	33.24	3.00
A2	38.10	3.27	1.36	6.10	7.45	36.73	2.68
A3	38.10	2.93	0.72	4.68	17.5	38.75	5.08
B1	19.05	3.09	0.84	6.01	9.98	33.45	4.43
B2	19.05	2.91	1.08	5.52	8.28	34.75	3.09
B3	19.05	3.29	0.75	5.93	14.92	32.04	5.38
C1	11.48	2.92	0.73	4.48	2.94	41.98	5.00
C2	11.48	2.69	0.72	4.22	4.57	13.05	4.67
C3	11.48	3.57	1.20	6.41	5.82	8.91	3.38
D1	5.74	4.21	1.04	6.00	2.83	8.48	4.71
D2	5.74	3.38	0.97	4.71	2.33	5.48	4.10
D3	5.74	3.28	0.90	5.66	3.97	8.45	4.33

3.5. Engineering demand parameters

Fig. 5 shows a schematic representation of the expected uplift force–displacement response of the OSB sheathing-to-framing connections used to define engineering demand parameters of interest. The engineering demand parameters are quantified based on the experimental data in the following sections. The force–displacement response data were analyzed to compute the yield force F_{yield} and the associated yield displacement δ_{yield}, the peak force F_{peak} and the displacement at peak force δ_{peak} along with the Pre-F_{peak} displacement at $0.8\times F_{peak}$ noted as $\delta_{0.8F_{peak}}$ and the Post-F_{peak} displacement at $0.4\times F_{peak}$ noted as $\delta_{0.4F_{peak}}$. F_{yield} is computed following the procedure outlined by ASTM D5652-21 [22]. ASTM D5652-21 defines F_{yield} as the force in the experimentally derived force–displacement response that intercepts the shifted approximate linear elastic force–displacement response $F(\delta) = K \times (\delta - 0.05 \times D)$, where $K = \frac{0.4\times F_{peak} - 0.1\times F_{peak}}{\delta_{II} - \delta_{I}}$ is the estimated elastic stiffness of the connection. The offset $0.05D$ in the calculation of F_{yield} is based on ASTM D5652-21, Section 10 [22]. The experimental data is used to compute the evolution of the tangent stiffness K_t. The three-dimensional displacement and strain results are quantified at V_{NDS}, F_{yield} and F_{peak}, the pre-peak force response at $0.8\times F_{peak}$, and the post-peak force response at $0.4 \times F_{peak}$.

4. Discussion

4.1. Force–displacement responses

Fig. 6 shows the force–displacement response curves along with the points on the force–displacement responses associated with F_{yield}, F_{peak}, and $0.4F_{peak}$. Table 1 lists the target edge distance, and the values of F_{yield}, δ_{yield}, F_{peak}, δ_{peak}, $\delta_{0.4F_{peak}}$, K for each specimen. The results show limited sensitivity of F_{yield}, δ_{yield} and K to the edge distance. A relatively large reduction of force was observed in Test Groups A and B after the Specimens reached F_{peak} followed by a plateau in the force–displacement response associated with approximately zero stiffness. Fig. 7 shows the average force–displacement response curves for each Test Group. The next section provides a discussion on the evolution of damage with the goal of explaining the effect of edge distances on the type of failure mode observed at the end of the tests and the values of δ_{peak} and $\delta_{0.4F_{peak}}$.

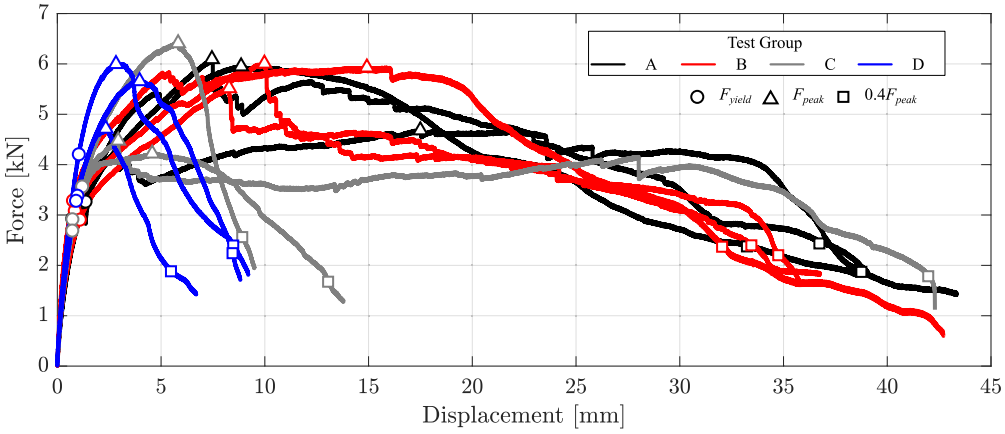


Fig. 6. Force and displacement responses.

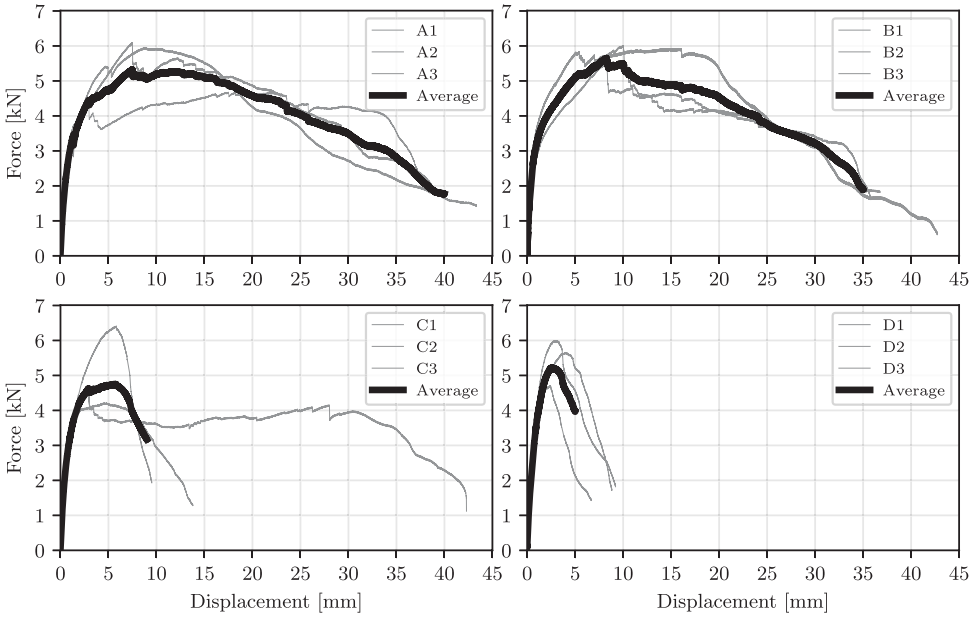


Fig. 7. Average force and displacement responses for each Test Group.

4.2. Evolution of damage

The spatial distribution of engineering strain and out-of-plane displacement was studied to further understand the evolution of damage in the nailed connections. Fig. 8 shows the evolution of the engineering principal strain for Specimens B2, B3, C2, C3, D2, and D3. DIC data from Specimens A, B1, C1, and D1 were omitted for conciseness. The engineering principal strain computed on the external face of the OSB panel were localized in the region of the nails. The magnitude of the engineering principal strain was negligible at a displacement associated with uplift force values equal to V_{NDS}. At δ_{yield}, initiation of strain localization was observed in the areas where the nails are positioned. The strain localization increases in all specimens for displacement levels equal or greater than $\delta_{0.8F_{peak}}$. The magnitude and the distribution of engineering strain was not uniform among the nails in a connection. Construction parameters such as the alignment of nails with respect to the target edge distance, and the actual nail edge distance resulted in variations in the distribution of the uplift force in each nail which in turn results in non-uniform strain localization in the regions with nails. The evolution of strain localization in the connections is discussed in the following sections. Emphasis is placed on the actual edge distance.

Fig. 9 shows the evolution of the engineering strain along the vertical direction of the uplift force, noted as ϵ_{yy}, focusing on Nail 2 and Nail 4 in Specimens B2, B3, C2, C3, D2, and D3. The magnitude of ϵ_{yy} in the contour plots was limited to 5×10^{-3} mm/mm for increased fidelity in the observations associated with uplift displacements less than or equal to $\delta_{0.8F_{peak}}$. The magnitude of ϵ_{yy} was

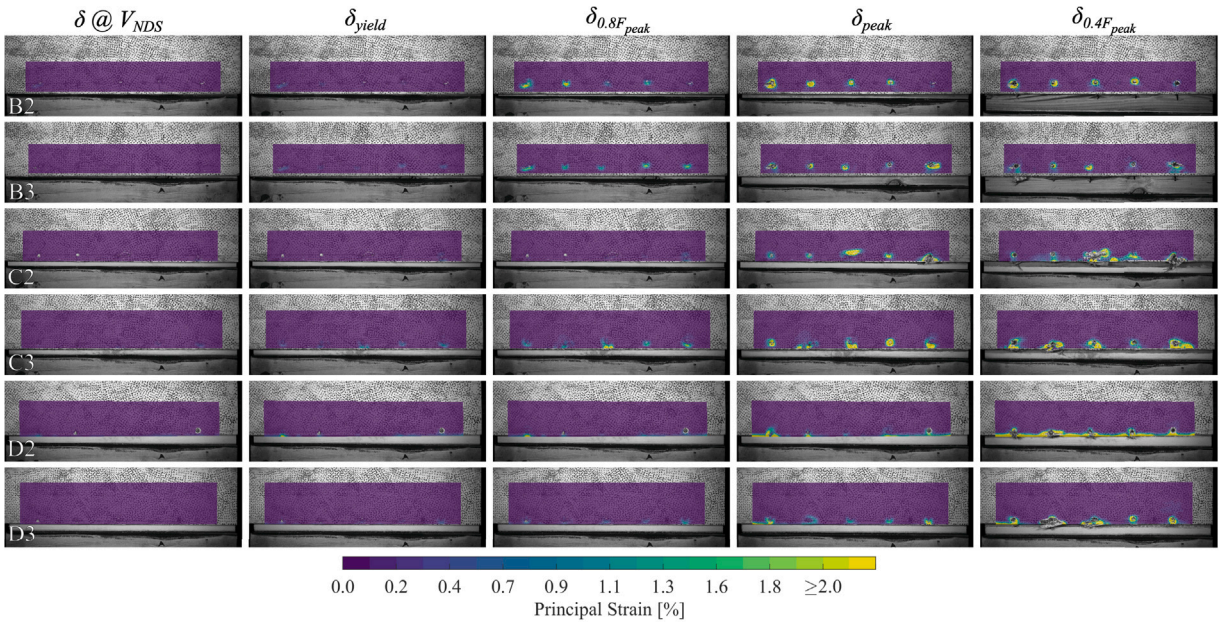


Fig. 8. Principal engineering strain in the external face of the OSB sheathing-to-framing nailed connections for selected Specimens in Test Groups B, C, and D.

less than or equal to 0.5% for uplift displacement less than or equal to δ_{yield}. The magnitude of ϵ_{yy} was practically similar above and below the nail head. The distribution of ϵ_{yy} above and below the nail head indicates that ϵ_{yy} develops primarily due to the bearing interaction between the nail head bottom surface and the OSB panel surface as the OSB panel was pulling the nail. Bearing failure of the OSB panel was observed in Test Groups C and D at $\delta_{0.4F_{peak}}$. Significant nail penetration of the nail through the thickness of the OSB panel was observed in Test Groups A and B at $\delta_{0.4F_{peak}}$.

Fig. 10 shows the evolution of the out-of-plane displacement in Specimens B2, B3, C2, C3, D2, and D3. Large out-of-plane displacement was observed in Specimens in Test Group B compared to the Specimens in Test Groups C and D. Relatively large out-of-plane displacement occurred in Specimens in Test Group B because of the kinematics enforced by the splitting of the sill plate perpendicular to the wood grain. Fig. 11 shows the out-of-plane displacement in Specimens B2, B3, C2, C3, D2, and D3 focusing on Nail 2 and Nail 4. The magnitude of the contour values was limited to 0.2 mm and 1 mm for the results below $\delta_{0.8F_{peak}}$ and above $\delta_{F_{peak}}$, respectively. A small gradient of out-of-plane displacement was observed for uplift displacements less than or equal to δ_{yield}. The small out-of-plane displacements at this uplift displacement level justified the small values of ϵ_{yy} observed in Fig. 9. At δ_{peak} the gradient of out-of-plane displacement increased, resulting in an out-of-plane rotation of the OSB panel in the range of 0.02 radians to 0.03 radians.

4.3. Yield mechanism and estimate of the yield force

The experimental results indicate that the yield mechanism is effectively independent of the edge distance. The yield mechanism of the connections considering the engineering strain and displacement field data is discussed in this section. Simple computations introduced by Johansen [23] were used to estimate the yield force in the nailed connections independent of the nail edge distance. The yield mechanism assumes the formation of a plastic hinge in the nail as shown in Fig. 12. The kinematic compatibility between the deformed nail and the OSB panel results in a deformed connection configuration as shown in Fig. 12. This schematic deformed shape reflects the out-of-plane displacement and engineering strain data shown in Fig. 12. Assuming plane sections remain plane, a linear variation of vertical engineering strain ϵ_{yy} was assumed through the thickness of the OSB panel. On the external face of the OSB panel $\epsilon_{yy} \leq 0.5\%$ was expected. Thus, the normal stress at the external face of the OSB panel was expected to be approximately below the dowel bearing strength $f_e = 32$ MPa [24] considering the modulus of elasticity of the OSB panel to be equal to $E_{OSB} = 5.3$ GPa [25]. The strain in the internal face of the OSB panel was assumed to be $\epsilon_{yy} > 0.5\%$. This assumption was made because the internal face of the OSB panel was expected to have reached the OSB dowel bearing strength when the nails yield in flexure. As a result, the bearing stress on the nail was expected to be approximately equal to the dowel bearing strength of the OSB panel within a distance $z_{M_{max}}$ away from the internal face of the OSB panel. The internal bending moment required for the nail to reach its normal yield stress due to an uplift force F_{ym} (i.e., force required to form the yield mechanism) was computed as $M_{yb} = \frac{f_{yb} \times \pi \times D^3}{32}$, where the normal yield stress of the nail was $f_{yb} = 732$ MPa [24] and nail diameter was $D = 2.87$ mm. The nail bearing stress was used to compute the internal shear force and internal bending moment in the nail within the thickness of the OSB panel t_{OSB}. The maximum internal shear and the maximum internal bending moment are computed as $V_{max} \equiv F_{ym} = f_e \times D \times z_{M_{max}}$

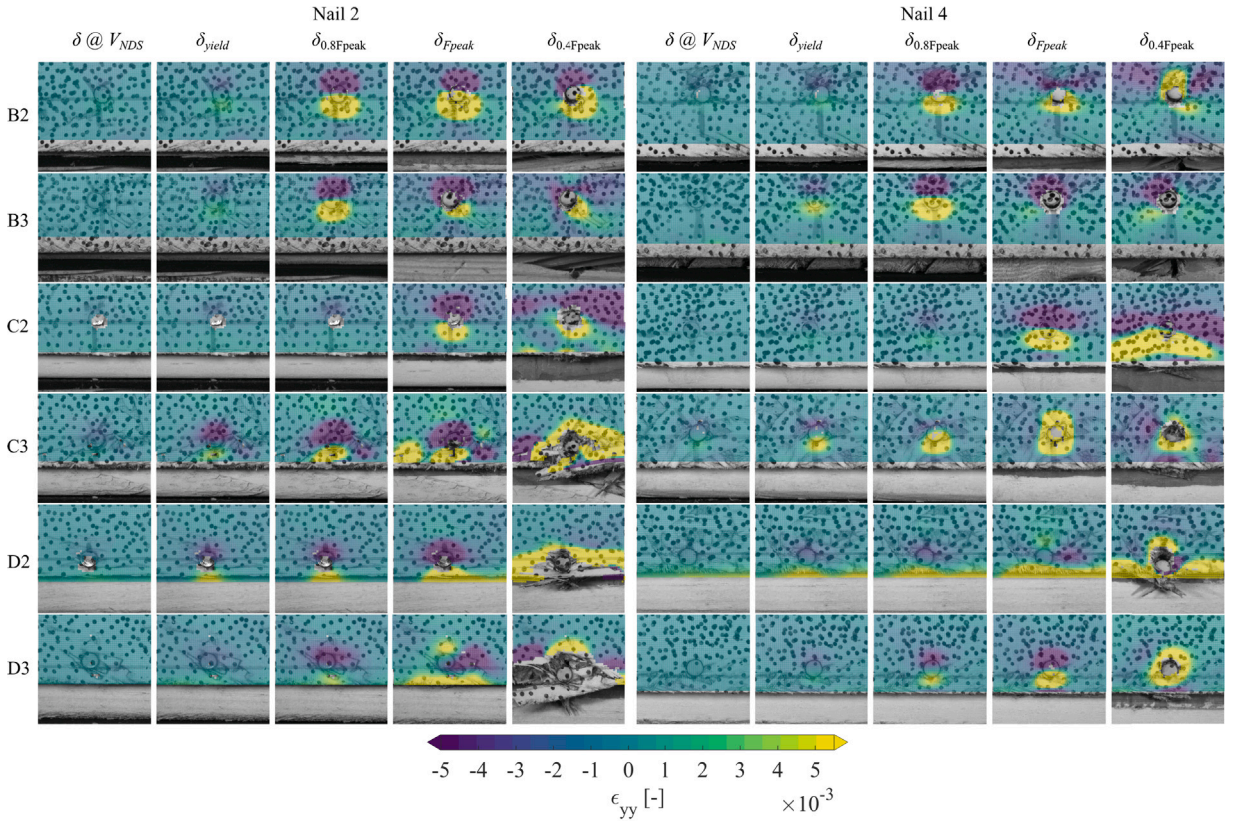


Fig. 9. Evolution of localized damage and vertical engineering strain in representative nail regions for selected Specimens in Test Groups B, C, and D.

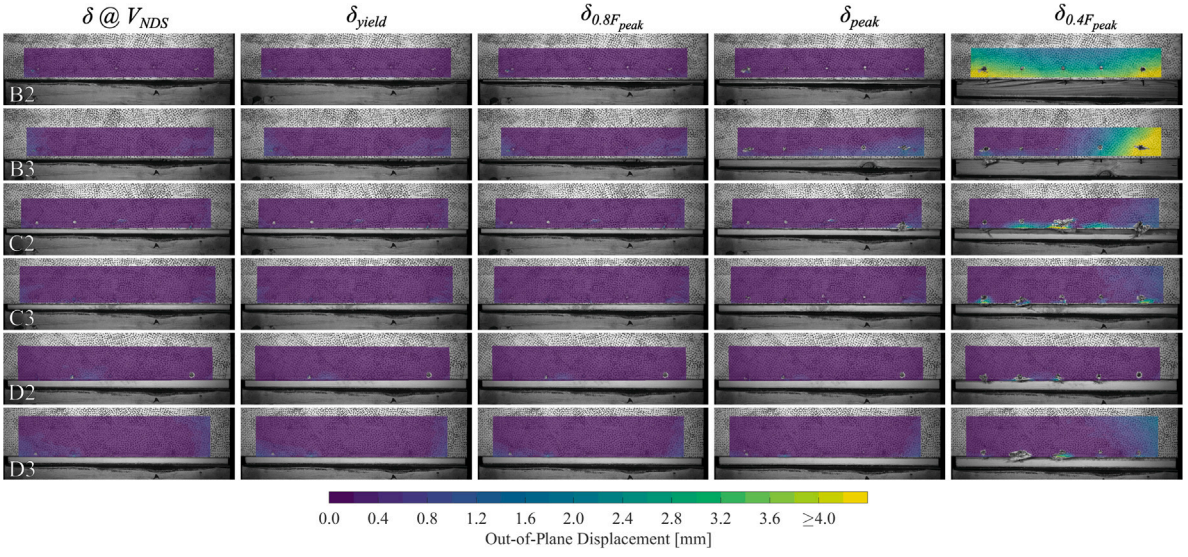


Fig. 10. Out-of-plane displacement in the external face of the OSB sheathing-to-framing nailed connections for selected Specimens in Test Groups B, C, and D.

and $M_{max} = \frac{F_{ym} \times z_{M_{max}}}{2} = \frac{F_{ym}^2}{2 \times f_e \times D}$, respectively. By equating the maximum internal bending moment with the nail yield bending moment the uplift force that results in the yield mechanism was computed as $F_{ym} = D^2 \times \sqrt{\frac{\pi}{16} \times f_e \times f_{yb}} = 0.56$ kN. Assuming a perfect geometry in which the uplift force was distributed equal to all nails, an estimated yield force that was independent of the nail edge distance was computed for the connections with five nails as $F_{ym,total} = 5 \times F_{ym} = 2.8$ kN.

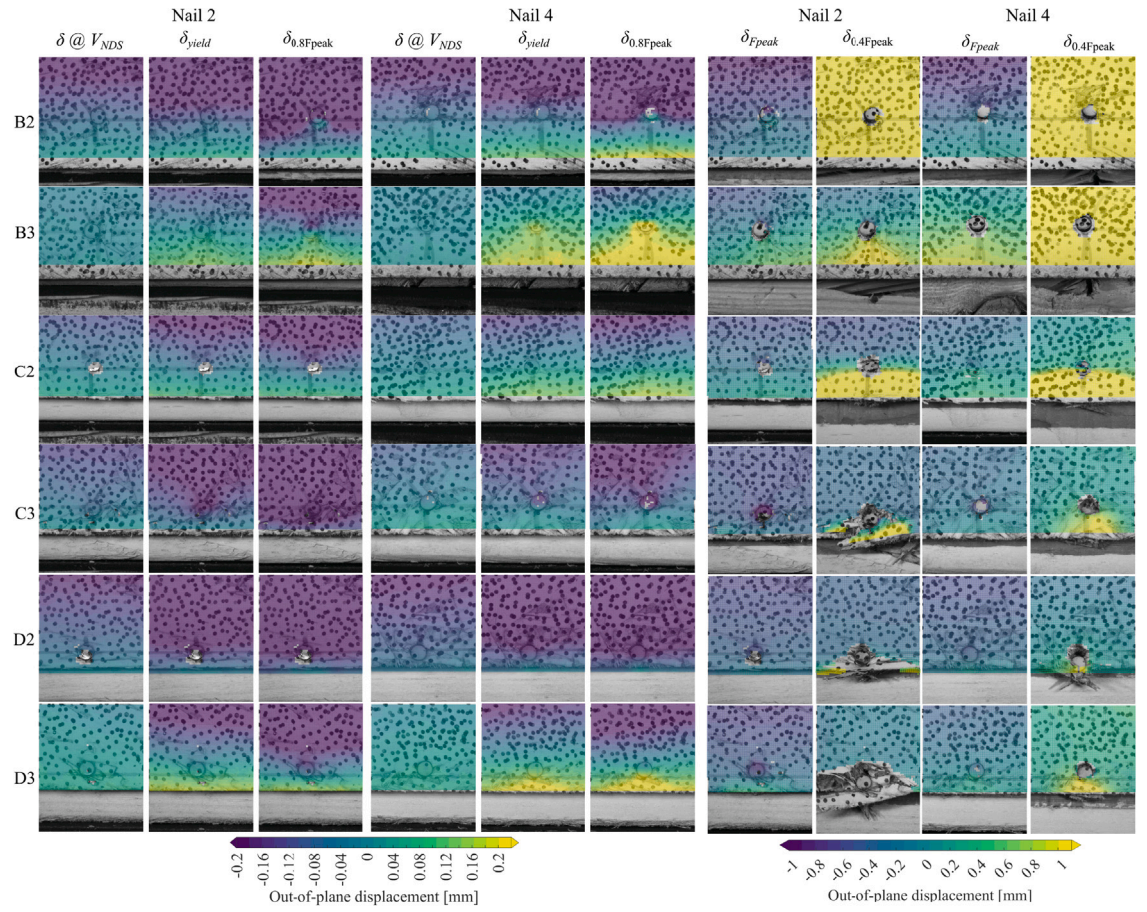


Fig. 11. Close up view of the evolution of out-of-plane deformation in representative nail regions for selected Specimens in Test Groups B, C, and D.

4.4. Post-yielding force–displacement response and failure mechanisms

Fig. 13 shows the force–displacement response observed in Specimens B2 and D2. The gray markers indicate the yield point based on F_{yield}. The white markers indicate the point in the force–displacement response when the force was equal to $0.8F_{peak}$. The black markers indicate a point in the force–displacement response right after F_{peak} was reached (i.e., Post-F_{peak}). The vertical engineering strain ϵ_{yy} in Specimens B2 and D2 is shown for $0.8F_{peak}$ and Post-F_{peak}. The post-yielding response in specimen B2 was associated with lower K_t and larger $\Delta\delta = \delta_{peak} - \delta_{yield}$ compared to specimen D2. This observation was attributed to the formation of second plastic hinges in the nails in specimen B2. The abrupt reduction in the force response of specimen B2 at Post-F_{peak} was associated with the initiation of the sill plate splitting due to the bearing load acting from the nails perpendicular to the grain of the wood of the sill plate. Initiation of significant penetration of Nail 1 and Nail 4 through the thickness of the OSB sheathing panel was observed. The large Post-F_{peak} inelastic displacement capacity in specimen B2 was associated with the inelastic deformation capacity of the nails that have not experienced significant nail penetration (e.g., specimen B2 Nail 2). The nails in the Specimens that sill plate splitting was observed at the end of the test had a deformed shape with a double curvature. The increased edge distance enables the formation of a double curvature in the deformed shape of the nails which resulted in relatively large $\delta_{0.4F_{peak}}$. Fig. 14 summarizes the sill plate failure mechanism with sketches and images captured at the end of a test. Sill plate splitting and penetration of the nails through the OSB panel defines the sill plate failure mechanism. The sill plate failure mechanism was observed in all Specimens in Test Groups A and B, and in Specimen C1.

The initiation of the reduction in the force response of Specimen D2 at Post-F_{peak} (Fig. 13) was associated with the initiation of the bearing failure of the OSB sheathing panel in Nail 1. By comparing the strain state in Nail 2 at $0.8F_{peak}$ and Post-F_{peak}, it can be observed that the OSB failure initiated at Nail 1 led to redistribution of the load which increased the strain in the OSB panel close to Nail 2. The nails in specimens that OSB failure was observed had a deformed shape with a single curvature. The OSB failure does not allow the formation of second plastic hinge in the nails. The bearing failure of the OSB panel at every nail defined the OSB failure mechanism. The OSB failure was observed in all specimens in Test Group D and in Specimens C2 and C3.

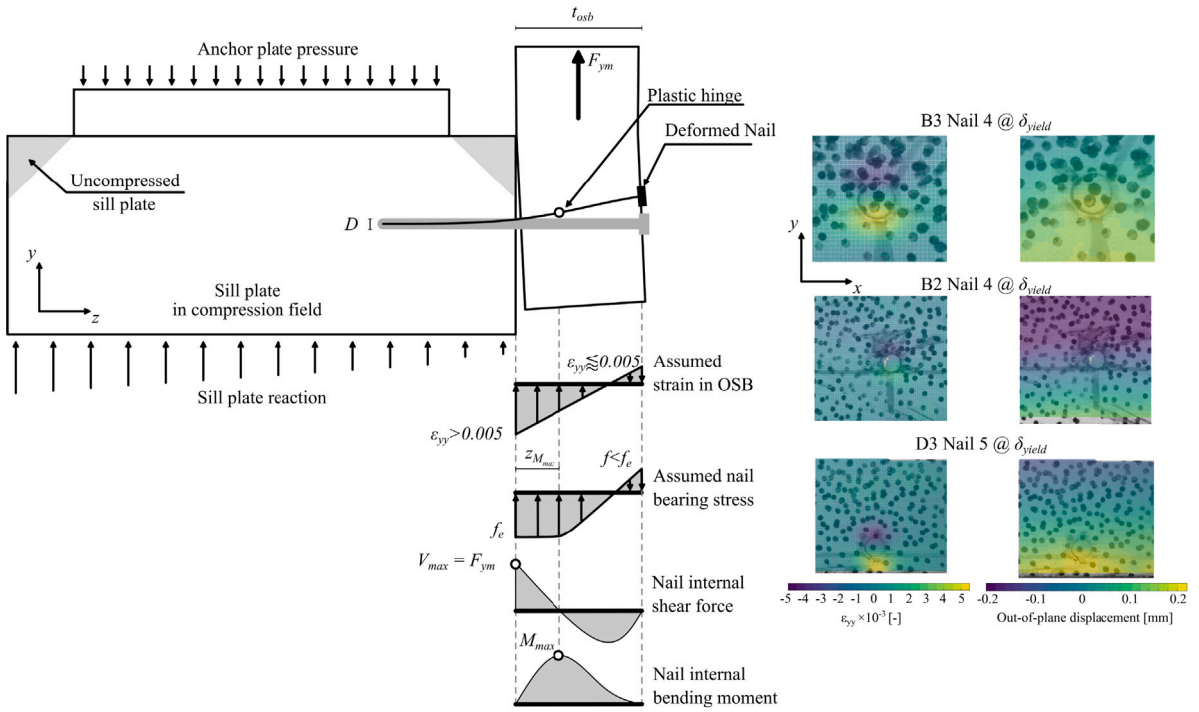


Fig. 12. Approximation of the yield force.

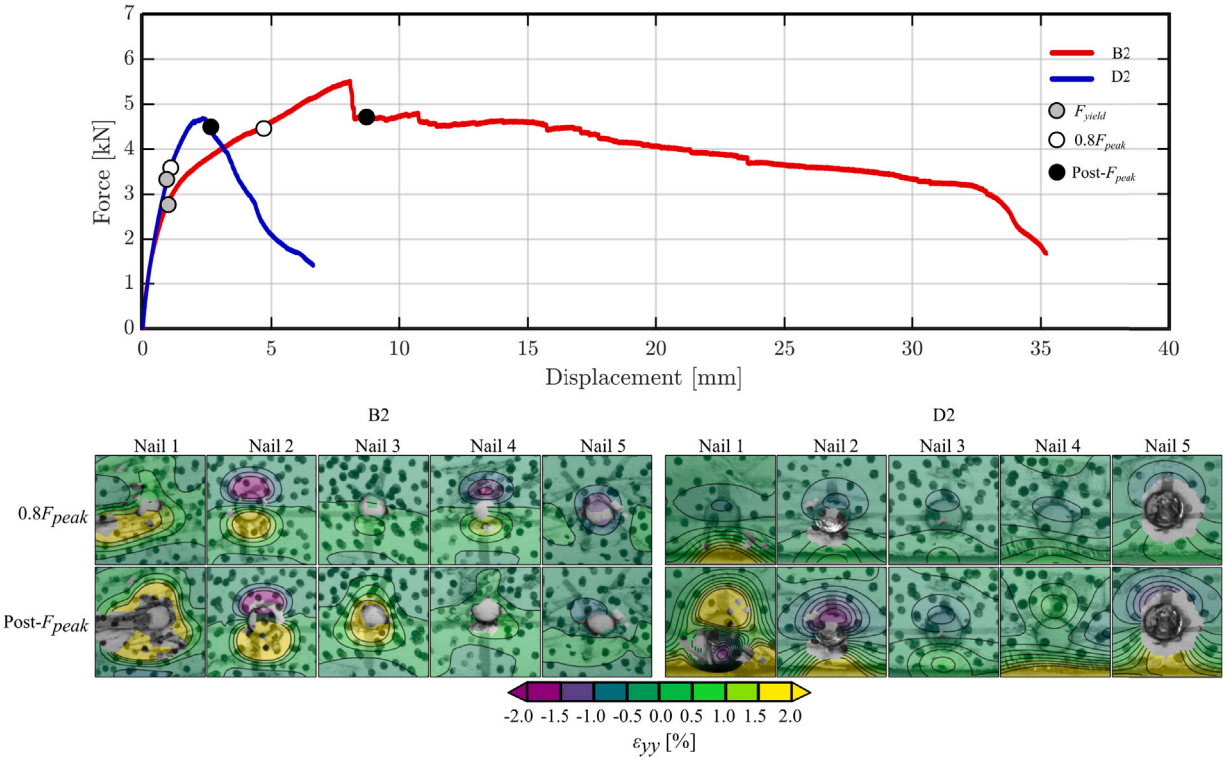


Fig. 13. Post-yielding force–displacement response and two observed mechanisms that contribute to the initiation of force degradation.

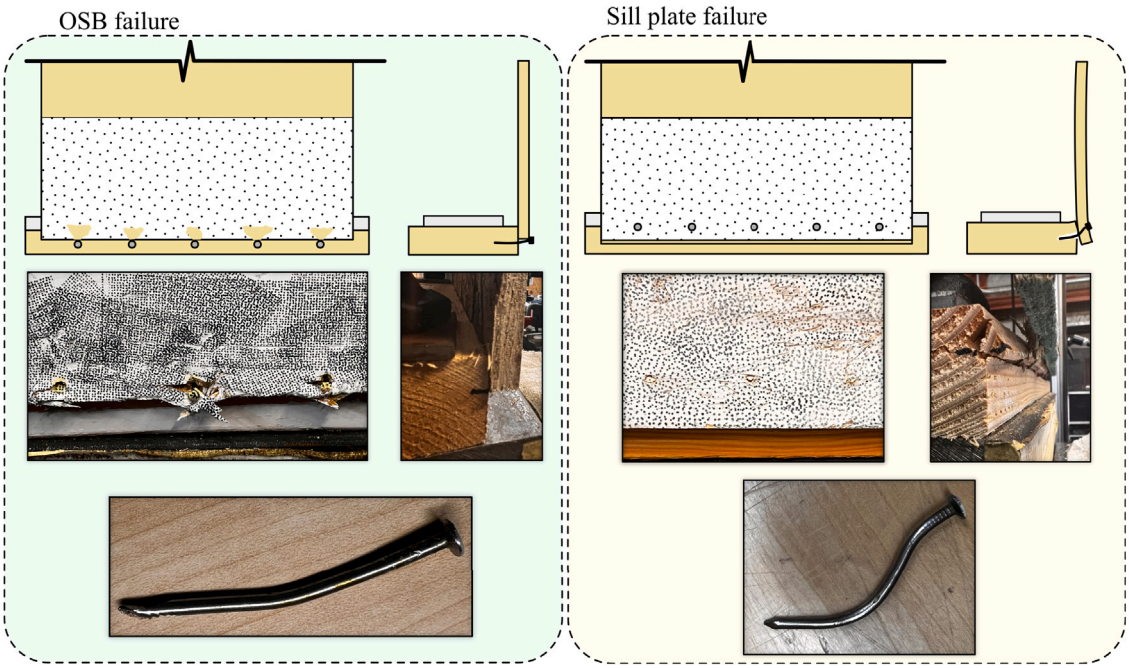


Fig. 14. Nail edge distance dependent failure mechanisms observed at the end of the tests.

4.5. Effect of edge distance on uplift-induced responses

Fig. 15(a) through (i) show the values of F_{yield}, δ_{yield}, F_{yield}/V_{NDS}, F_{peak}, δ_{peak}, F_{peak}/F_{yield}, K, $\delta_{0.4F_{peak}}$, and $\delta_{peak}/\delta_{yield}$ with respect to the edge distance in each Test Group, respectively. $F_{ym,total}$ is compared to F_{yield} for each Test Group. Table 2 lists the edge distance and mean values (μ) of F_{peak}, δ_{peak}, F_{yield}, δ_{yield}, $\delta_{0.4F_{peak}}$, and K for Test Groups B, C, and D, noted as $\mu_{F_{peak}}$, $\mu_{\delta_{peak}}$, $\mu_{F_{yield}}$, $\mu_{\delta_{yield}}$, $\mu_{\delta_{0.4F_{peak}}}$, and μ_K, normalized by the mean values for Test Group A $\mu_{F_{peak,A}}$, $\mu_{\delta_{peak,A}}$, $\mu_{F_{yield,A}}$, $\mu_{\delta_{yield,A}}$, $\mu_{\delta_{0.4F_{peak,A}}}$, and $\mu_{K,A}$.

The values of $\mu_{F_{peak}}/\mu_{F_{peak,A}}$ and $\mu_{\delta_{peak}}/\mu_{\delta_{peak,A}}$ were between 0.98 and 1.15. $F_{ym,total}$ approximated reasonably well a lower bound of F_{yield}, with F_{yield} typically being larger than $F_{ym,total}$. This observation was attributed to the fact that $F_{ym,total}$ was computed assuming construction without imperfections (i.e., perfect alignment of all five nails) which resulted in all nails reaching M_{yb} at the same value of δ. However, due to construction imperfections the deformation of each nail varies at any given δ and the expected load transferred through each nail was not the same. This observation was supported by the variation in the magnitude of engineering strain near the head of the nails. As a result, the nails reached M_{yb} at the different values of δ. As δ increased, the nails progressively reached M_{yb}. As δ increased, strain hardening was expected in the nails that have already yielded. Thus, $F_{yield} \geq F_{ym,total}$ when all nails have reached at least M_{yb}. Furthermore, variation in the steel material properties of the nails may have also contributed to the variation of the F_{yield} compared to $F_{ym,total}$ which assumed a deterministic estimated value for the nail normal yield stress f_{yb}. With respect to the yielding response, it was also observed that μ_K is approximately 20% larger in Test Groups B, C, and D compared to Test Groups A (Fig. 15(g)). It is acknowledged that the relatively large variability in values of K results in low statistical confidence. The computation of accurate statistical quantities that can be used for the derivation of probability density functions of the engineering demand parameters is outside the scope of this study. Despite this fact, the data indicate that small edge distances associated with OSB failure may result in more consistent values of K compared to larger edge distances associated with sill plate failure.

Fig. 15(c) shows that the ratio F_{yield}/V_{NDS} was similar for Test Groups A, B, and C and increased above 3.0 for Test Group D. It was noted that V_{NDS} for Test Group D was computed considering a reduction factor of 1/2 to account for the reduced edge distance. As a result, a design safety factor against the actual yield force of approximately 1.5 or higher can be expected independently of the edge distance. This result could contribute toward the increased confidence in the design of OSB sheathing-to-framing connections relative to construction imperfections related to nail edge distances smaller than the minimum nail edge distances required by NDS.

An increased variability in F_{peak} (Fig. 15(d)) and δ_{peak} (Fig. 15(e)) values was observed compared to the yield values. Despite the increased variability, $\mu_{F_{peak}}$ in Test Groups B, C, and D was similar to $\mu_{F_{peak,A}}$ within 10% difference. The edge distance significantly affects δ_{peak} and $\delta_{0.4F_{peak}}$ (Fig. 15(h)). Relatively large δ_{peak} and $\delta_{0.4F_{peak}}$ were observed in Test Groups A and B compared to Test Groups C and D. The difference was justified through the observed post-yielding force–displacement response and the failure mechanisms discussed in the previous section. The relatively large deformation capacity in Test Groups A and B in which sill plate failure was observed was attributed to the double curvature and double plastic hinge formation in the nails. In structural wall

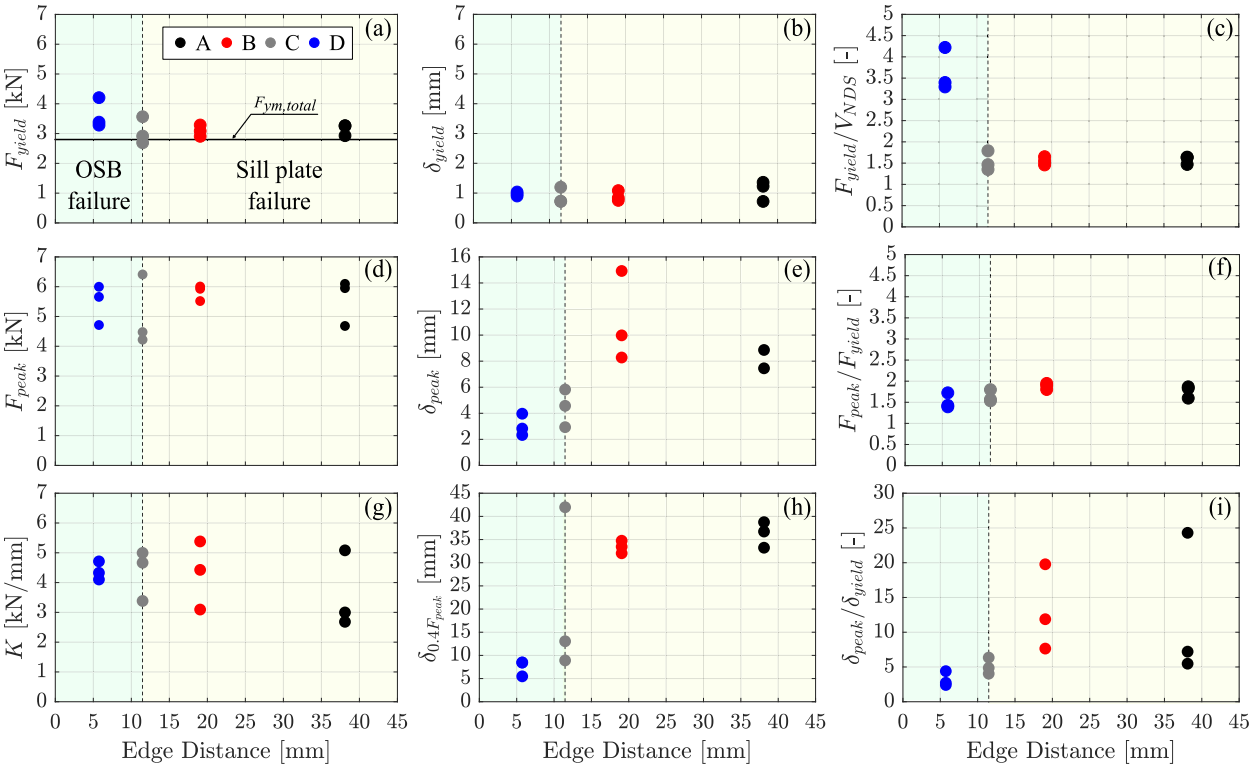


Fig. 15. Response quantities with respect to edge distance.

Table 2
Edge distance and mean response quantities for Test Groups B, C, and D normalized by the quantities of Test Group A, Edge distance group A = 38.10 mm, $\mu_{F_{peak,A}} = 5.58$ kN, $\mu_{\delta_{peak,A}} = 11.27$ mm, $\mu_{F_{yield,A}} = 3.15$ kN , $\mu_{\delta_{yield,A}} = 1.10$ mm, $\mu_{\delta_{0.4F_{peak},A}} = 36.24$ mm, $\mu_{K_A} = 3.59$ kN/mm.

Test Group	$\frac{\text{Edge distance}}{\text{Edge distance group A}}$	$\frac{\mu_{F_{yield}}}{\mu_{F_{yield,A}}}$	$\frac{\mu_{\delta_{yield}}}{\mu_{\delta_{yield,A}}}$	$\frac{\mu_{F_{peak}}}{\mu_{F_{peak,A}}}$	$\frac{\mu_{\delta_{peak}}}{\mu_{\delta_{peak,A}}}$	$\frac{\mu_K}{\mu_{K_A}}$	$\frac{\mu_{\delta_{0.4F_{peak}}}}{\mu_{\delta_{0.4F_{peak},A}}}$
[–]	[–]	[–]	[–]	[–]	[–]	[–]	[–]
B	0.50	0.98	0.81	1.04	0.98	1.20	0.92
C	0.30	0.97	0.80	0.90	0.39	1.21	0.59
D	0.15	1.15	0.88	0.98	0.27	1.22	0.21

assembly systems, redistribution of forces should be expected prior of reaching the relatively large δ_{peak} and $\delta_{0.4F_{peak}}$ displacements observed in Test Groups A and B.

Fig. 15(f) shows the approximate range $F_{peak}/F_{yield} \in [1.5, 2.0]$. The ratio F_{peak}/F_{yield} is a measure of peak force capacity in the nailed connections relative to their yield force capacity. This indicates that as the edge distance increased the F_{peak}/F_{yield} increased. $\delta_{peak}/\delta_{yield}$ is a measure of ductility in the nailed connections. Fig. 15(i) shows that as the edge distance increased the ratio $\delta_{peak}/\delta_{yield}$ increased. The variability of the ratios $\delta_{peak}/\delta_{yield}$ increased as the edge distance increased, as well. $\delta_{peak}/\delta_{yield}$ was greater than or equal to 2.0 in all specimens. The variability in $\delta_{peak}/\delta_{yield}$ computed based on the results from Test Groups A and B was larger compared to Test Groups C and D.

To further understand the evolution of stiffness of the connection as it transitions from elastic to post-elastic force–displacement response, the tangent stiffness K_t was computed at various values of δ for the specimens in each Test Group. An exponential function of K_t with respect to the normalized displacement δ/δ_{peak} was fitted to the data for each Test Group. Fig. 16 shows the fitted curves and the comparison of the evolution of the tangent stiffness K_t with respect to δ/δ_{peak} for the Test Groups A, B, C, and D. As mentioned earlier, the larger edge distance in Test Groups A and B was associated with larger δ_{peak} and more ductile force–displacement response compared to Test Groups C and D. As a result, K_t values for the Specimens in Test Groups C and D are appeared to be higher within the range of $\delta/\delta_{peak} \in [0.1, 0.4]$ compared to the Specimens in Test Groups A and B.

5. Summary and conclusions

In light-framed wood construction, sheathing edge nailing at laps plays a crucial role in uplift load transfer, ensuring that wind and seismic forces are effectively resisted. The precision of panelized construction allows for consistent edge distances, maximizing

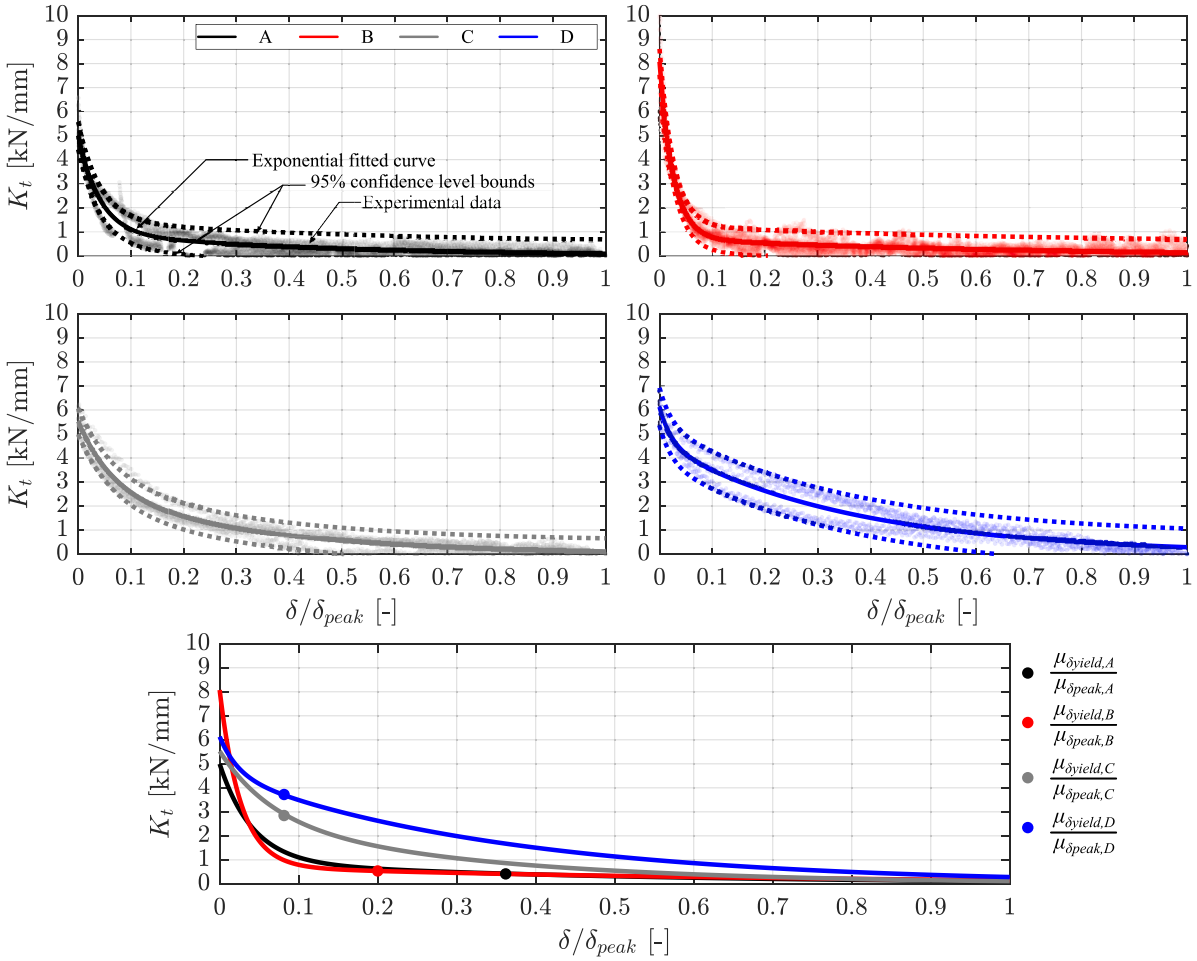


Fig. 16. Evolution of tangent stiffness K_t.

fastener performance and uplift load path continuity. However, field-built walls often introduce variability in nailing placement, which can result in reduced edge distances and potential loss of uplift capacity.

This paper characterized experimentally the effect of the distance between the OSB panel edge and the nails on the wind-induced uplift response of sheathing-to-framing nailed connections. Four edge distances were considered. Twelve sheathing-to-framing nailed connections were tested to failure. Analysis of the three-dimensional displacement and strain fields computed using state-of-the-art Digital Image Correlation (DIC) method was performed to provide insights into the force–displacement response, the yield mechanism, the post-yielding response, the failure mechanisms, and the evolution of stiffness of the connections. Detailed observations on the effect of the edge distance to the response of nailed connections useful to the structural engineering practice were provided. The experimental study concluded to the observations listed below:

- The variation of the nail edge distance has minimal effect on the simulated wind-induced uplift yield force, yield displacement, and peak force even for edge distances smaller than the minimum edge distances provided by NDS.
- The nail edge distance affects the displacement at peak force and the displacement at forty percent of the peak force.
- The yield mechanism of the connections is practically independent of the nail edge distance and a lower bound of the expected yield force can be computed using simple calculations.
- Effectively no strain localization and stiffness degradation was observed up to an uplift force equal to the uplift design force computed using NDS. No significant strain localization was observed up to the computed uplift yield force of the connections.
- Non-uniform strain localization at displacements larger than the yield displacement was observed. This observation was attributed to the variation in the distribution of the uplift force in each nail due to construction parameters such as the alignment of nails with respect to the target edge distance and the actual nail edge distance.
- Two failure modes were observed. Sill plate and OSB failure was observed in connections with larger and smaller nail edge distance, respectively. Due to the dual plastic hinge formation, sill plate failure mechanism resulted in higher ductility and slightly higher peak force compared to OSB failure.

- All tests resulted in yield force greater than the connections design force computed per NDS.

This study provides valuable insights into the effect of nail edge distance on the uplift response of sheathing-to-framing connections using a state-of-the-art DIC method, which enables accurate, full-field strain measurements. Future research could focus on additional testing with a larger sample size to enable the computation of probability density functions of the engineering demand parameters. Such statistical assessment can rely on simpler force and displacement data along with the increased number of specimens, eliminating the need for time-consuming DIC methods to compute detailed full-field strain data.

In addition, systematic wall system level studies could be performed to assess the impact of the localized effects studied in this manuscript on the global wall system level subjected to combined shear and uplift force effects.

CRediT authorship contribution statement

Georgios Tsampras: Writing – review & editing, Writing – original draft, Visualization, Validation, Supervision, Software, Resources, Project administration, Methodology, Investigation, Funding acquisition, Formal analysis, Data curation, Conceptualization. **Richard Zabel:** Writing – review & editing, Conceptualization. **Kaixin Chen:** Writing – review & editing, Investigation.

Declaration of competing interest

The authors declare that they have no known competing financial interests or personal relationships that could have appeared to influence the work reported in this paper.

Acknowledgments

The authors acknowledge the financial support provided by Mulhern and Kulp Residential Structural Engineering company, United States of America and the equipment and facilities resources made available by the Department of Structural Engineering at the University of California San Diego, United States of America. Any opinions, findings, and conclusions expressed in this paper are those of the authors and do not necessarily reflect the views of others acknowledged here.

Data availability

Data will be made available on request.

References

[1] J.T. Easley, M. Foomani, R.H. Dodds, Formulas for wood shear walls, ASCE J. Struct. Div. 108 (11) (1982) 2460–2478.
[2] J.D. Dolan, B. Madsen, Monotonic and cyclic nail connection tests, Can. J. Civ. Eng. 19 (1992) 97–104.
[3] A.J. Salenikovich, J.D. Dolan, The racking performance of shear walls with various aspect ratios. Part I. Monotonic tests of fully anchored walls, For. Prod. J. 53 (10) (2003) 65–73.
[4] A.J. Salenikovich, J.D. Dolan, The racking performance of shear walls with various aspect ratios. Part 2. Cyclic tests of fully anchored walls, For. Prod. J. 53 (11/12) (2003) 37–45.
[5] F.S. Fonseca, S.K. Rose, S.H. Campbell, Nail, wood screw, and staple fastener connections, 2002.
[6] S.N. Jones, F.S. Fonseca, Capacity of oriented strand board shear walls with overdriven sheathing nails, ASCE J. Struct. Eng. 128 (7) (2002) 898–907.
[7] S.M. Kent, R.J. Leichti, D.V. Rosowsky, J.J. Morrell, Effects of decay on the cyclic properties of nailed connections, J. Mater. Civ. Eng. 17 (5) (2005) 579–585.
[8] W. Seim, M. Kramar, T. Pazlar, T. Vogt, OSB and GFB as sheathing materials for timber-framed shear walls: Comparative study of seismic resistance, ASCE J. Struct. Eng. 142 (4) (2016).
[9] T. Sartori, R. Tomasi, Experimental investigation on sheathing-to-framing connections in wood shear walls, Eng. Struct. 56 (2013) 2197–2205.
[10] B. Folz, A. Filiatrault, Cyclic analysis of wood shear walls, ASCE J. Struct. Eng. 127 (4) (2001) 433–441.
[11] L. Zhou, Y.-H. Chui, C. Ni, Influence of middle member thickness on properties of double-shear nail joints, ASCE J. Struct. Eng. 144 (8) (2018).
[12] T.K. Bader, J. Vessby, B. Enquist, Path dependence in OSB sheathing-to-framing nailed connection revealed by biaxial testing, ASCE J. Struct. Eng. 144 (10) (2018).
[13] D. Way, A. Sinha, F.A. Kamke, Performance of light-frame timber shear walls produced with weathered sheathing, ASCE J. Archit. Eng. 26 (1) (2020).
[14] M. Spasojevic, H. Daneshvar, Y. Chen, Y.H. Chui, Lateral resistance of sheathing-to-framing nailed joints with an intermediate insulation layer, ASCE J. Struct. Eng. 147 (6) (2021).
[15] American Wood Council, National design specification for wood construction, 2018.
[16] American Wood Council, Special Design Provisions for Wind and Seismic (SDPWS), Leesburg, VA, 2021.
[17] H. Schreier, J.-J. Orteu, M.A. Sutton, Image Correlation for Shape, Motion and Deformation Measurements: Basic Concepts,Theory and Applications, Springer US, Boston, MA, 2009, http://dx.doi.org/10.1007/978-0-387-78747-3.
[18] MTS, MTS TestSuite software, 2024.
[19] Correlated Solutions, Correlated solutions digital image correlation, 2024, URL: https://www.correlatedsolutions.com,
[20] MathWorks, MATLAB Version: 23.2.0 (R2023b), The MathWorks Inc., Natick, Massachusetts, United States, 2023, URL: https://www.mathworks.com.
[21] G. Van Rossum, Python programming language, 2024, URL: https://www.python.org/.
[22] ASTM, ASTM D5652: Test Methods for Single-Bolt Connections in Wood and Wood-Based Products, ASTM International, D07 Committee, 2021, http://dx.doi.org/10.1520/D5652-21.
[23] K.W. Johansen, Theory of timber connections, Int. Assoc. Bridg. Struct. Eng. (9) (1949) 249–262.
[24] American Wood Council, General dowel equations for calculating lateral connection values, 2015.
[25] R. Ross, Wood Handbook—Wood as an Engineering Material, U.S. Department of Agriculture, 2021.